The CNS lymphatic system modulates the adaptive neuro-immune response in the perilesional cortex after brain trauma

Wojciechowski Sara[1], Vihma Maria[2], Galbardi Barbara[3], Keuters Meike H.[1,2], Antila Salli[4], Koistinaho Jari[2,1] and Noe Francesco M.[2]*

[1]A.I. Virtanen Institute for Molecular Sciences, University of Eastern Finland, 70210 Kuopio, Finland

[2]Neuroscience Center, Helsinki Institute of Life Science (HiLIFE), University of Helsinki, 00290 Helsinki, Finland

[3]Breast Cancer Unit, Department of Medical Oncology, IRCCS Ospedale San Raffaele, 20132 Milano, Italy

[4]Wihuri Research Institute and Translational Cancer Biology Program, Biomedicum Helsinki, University of Helsinki, 00290 Helsinki, Finland

Keywords: Controlled Cortical Impact (CCI), traumatic brain injury, CD8+ T lymphocytes, resident memory T cells, deep cervical lymph nodes.

Abstract

Rationale: The recently discovered meningeal lymphatic vessels (mLVs) have been proposed to be the missing link between the immune and the central nervous systems. The role of mLVs in modulating the neuro-immune response following a brain injury, however, has not been analyzed. Parenchymal T lymphocyte infiltration has been previously reported as part of secondary events after traumatic brain injury (TBI), suggestive of an adaptive neuro-immune response. The phenotype of these cells has remained uncharacterized. In this study, we identified the subpopulations of T cells infiltrating the perilesional areas 30 days post-injury (an early-chronic time point). Furthermore, we analyzed how the lack of mLVs affects the magnitude and the type of immune response in the brain after TBI. *Methods*: TBI was induced in K14-VEGFR3-Ig mice (lacking mLVs), or in their littermate controls (WT), applying a controlled cortical impact (CCI). One month after TBI, T cells were isolated from cortical areas ipsilateral or contralateral to the trauma and from the spleen, and analyzed by flow cytometry for TCRβ (T cells), CD4 (T-helper

cells), CD8 (cytotoxic T cells), CD44 (memory T cells), and CD69 (effector T cells). Lesion size in each animal was evaluated by MRI. *Results*: In both WT- and K14-VEGFR3-Ig-CCI mice, we found a prominent T cell infiltration in the brain, confined to the perilesional cortex and hippocampus. The majority of infiltrating T cells are CD8+ (cytotoxic T cells), expressing a $CD44^{hi}CD69+$ phenotype, suggesting that these are effector resident memory T cells. K14-VEGFR3-Ig mice showed a significant reduction of infiltrating CD4+ T lymphocytes, implying that mLVs are important in establishing a proper neuro-immune response. Negligible T cell infiltration was observed in the contralateral unaffected side. Extension of the lesion (measured as lesion volume from MRI) did not differ between the genotypes. Finally, TBI did not correlate with alterations in peripheral circulating T cells, as assessed one month after injury induction. *Conclusions*: Our data support the hypothesis that mLVs are pivotal for a proper and specific neuro-immune response after TBI, which is principally mediated by the resident memory cytotoxic CD8+ T cells.

Introduction

Traumatic brain injury (TBI) is among the top causes of death and disability in adult life with an estimated incidence of 0.20-0.52 % in the general population (1, 2). Approximately 2 % of the population just in the USA suffer from a wide-range of lifelong physical and psychological invalidities caused by TBI (3).

TBI is defined as an alteration in brain function, or other evidence of brain pathology, caused by an external force (4), which results in immediate neuronal cell death, diffuse axonal injury, ischemia, and hemorrhage (5). These primary insults initiate a progressive cascade of secondary injuries, which include macrophage infiltration (6), neuro-inflammation (microglia and astrocyte activation associated with cytokine production), edema formation, oxidative stress, neuronal necrosis and apoptosis, and white matter atrophy (5). Secondary injuries can progress for years in patients and rodent models of TBI, and are the causes of the neurological and psychiatric deficits associated with the pathology (7).

Among secondary events following TBI, recruitment of peripheral immune cells into the brain, including T lymphocytes, has been described (8-10). Two distinct waves of infiltrating CD3+ T cells have been reported in the injured brain. First, a massive infiltration occurs immediately after trauma (peaking 3 days post-injury – dpi) (8). After one month, this is followed by a second recruitment, which persists chronically (10) (late adaptive immune response). However, the

mechanisms and the consequences of the activation of the adaptive immune system after TBI are still poorly understood.

A proper immune surveillance of the brain was long disputed (11), due to the lack of a classical lymphatic system within the central nervous system (CNS). However, recent studies have described the presence of anatomically distinct lymphatic vessels in the meninges surrounding the brain and the spinal cord (meningeal lymphatic vessels – mLVs), preferentially draining the cerebrospinal fluid into the deep cervical lymph nodes (dcLNs) (12-14). Within these secondary lymphoid organs, brain-derived antigens are presented to resident T lymphocytes, evoking different cellular fate and immune responses based on the inflammatory milieu. It has been demonstrated that dcLNs play a specific role in neuro-immune interaction, ensuring the protection of brain cells by promoting a non-cytotoxic immune response (15-17). From this prospective, mLVs and dcLNs are essential components of a putative specific CNS lymphatic system, and the mLVs could be essential in the activation of immune responses to brain insults, by transporting brain-derived antigens to the dcLNs.

The aim of our work was to better characterize the late adaptive immune response and to decipher the mechanisms underpinning the activation of T lymphocytes after TBI, focusing on the specific role of mLVs in this process. In this regard, we induced a cerebral contusion in the cortex of transgenic K14-VEGFR3-Ig mice that completely lack lymphatic vessels in several tissues, including the meninges (14, 18). We examined the phenotype of T lymphocytes infiltrating the perilesional cortical areas, determining the prevalence of a CD8+ mediated cytotoxic immune response in the TBI mice lacking the lymphatic system. One month after brain injury, infiltrating T lymphocytes and circulating peripheral T cell populations in the spleen were phenotyped by flow cytometry. MRI was used to evaluate and compare lesion size in both transgenic animals and in their wild type littermates.

Our data show that the CNS immune response after TBI is specific and independent from peripheral immune activation. We also demonstrate that the lack of a functional mLVs-dcLNs connection alters the neuro-immune interaction after TBI, specifically dampening the CD4+ mediated immune response. No differences in MRI cortical lesion were found between the two genotypes. Finally, independent of genotype, infiltrating T cells present an effector phenotype, supporting their role in secondary injuries after TBI.

Material and Methods

Mice

Initial breeding pairs of K14-VEGFR3-Ig mice (C57BL/6JOlaHsd background (18)) were developed by Prof. K. Alitalo at University of Helsinki, and the colony was further expanded and maintained at University of Eastern Finland (Kuopio, Finland). Wild type (WT) and transgenic K14-VEGFR3-Ig mice used in all the experiments were littermates. Genotype screening was routinely confirmed by polymerase chain reaction analysis of ear punch samples. Mixed WT and K14-VEGFR3-Ig mice were housed in standard laboratory cages (four animals per cage, until surgery) in a controlled enriched environment (constant temperature, 22 ± 1 °C, humidity 50–60 %, lights on 07:00–19:00), with food and water available ad libitum (19). After TBI induction, mice were kept two per cage, separated by a pierced partition. All animal procedures were approved by the Animal Ethics Committee of the Provincial Government of Southern Finland and performed in accordance with the guidelines of the European Community Council Directives 2010/63/EU.

Controlled cortical Injury (CCI) mouse model of TBI

All surgical procedures were performed aseptically whenever possible.

Adult male mice (5 months old) were deeply anesthetized with isoflurane (5 % for induction, 1.0-1.5 % for maintenance, in 0.5 L/min air; see Supplementary Table 1), and the heads fixed to a stereotaxic frame (Kopf, Tujunga, USA). The scalp was shaved and then scrubbed (3x) with alternating Betadine (povidone-iodine 10 %) and 70 % ethanol, and local anesthesia of Xylocain gel (2 % solution) was applied. After skull exposure, a 5 mm circular craniotomy was manually drilled over the left parieto-temporal cortex, with the posterior edge of the craniotomy opposed to the lambdoid suture and the right edge to the sagittal suture. In order to reduce heating during manual craniotomy, the skull was irrigated with cold 0.9 % saline solution. The carved bone was carefully removed, without disrupting the underlying dura, and placed in 1 % Betadine solution. Thereafter, the animal was disconnected from isoflurane anesthesia for 5 min (stage 3 plane 1 according to Guedel's classification (20)), and CCI was induced using an electromagnetic stereotaxic impact actuator (ImpactOne, Leica, Richmond, VA, USA). The 3 mm blunt tip of the impactor was adjusted to the center of the exposed dura perpendicular to the brain surface, and the impact was administered at a depth of 0.5 mm, a speed of 5.0 m/s, and dwell time of 100 ms. The total duration of the craniotomy procedure including anesthesia induction was 35-40 min (Supplementary Table 1). After the impact, the mouse was reconnected to the isoflurane system, and the removed skull was returned to its original position and secured with bone cement (Selectaplus + Palacos R+G 50/50). The scalp was sutured (the total duration of post-impact surgery was 10 min), and treated

with Cicatrene powder (Neomycin + Bacitracin) and Terramycin spray (Oxytetracycline). The mice were injected i.p. with 1 mL pre-warmed sterile saline (35 ºC), and allowed to fully recover in an incubator at 32 ºC.

Craniotomy-related neuroinflammation has been previously reported in this model and the craniotomy itself can be considered a form of minor brain trauma (21). However, the contribution of these surgery-induced brain damages to the pathophysiology of TBI, and specifically to the induced neuro-immune response, has no clinical relevance. Due to the fact that the aim of our study is to characterize the adaptive immunity in response to a mild TBI, and not to analyze how differences in trauma severity can affect the neuro-immune response, in compliance to the 3R principle, we excluded the sham-operated animals from our study, and we used naïve mice not exposed to the surgical procedure as proper controls.

In vivo MRI and lesion volume definition

MRI data were acquired 21 days after TBI induction in a 7T horizontal magnet (Bruker Pharmascan, Ettlingen, Germany). Images were acquired using a four-channel mouse brain surface coil, a 3D T2-weighted Fast Spin-Echo sequence (RARE, repetition time 1.5 s, effective echo time 48 ms, 16 echoes per excitation) with 100 µm isotropic resolution (field of view 25.6 mm x 128.8 mm x 9.6 mm; acquisition matrix 128 x 256 x 96). Scans were performed with the mouse under 1.0-1.5 % maintenance isoflurane anesthesia (70/30 N2O/oxygen gas mixture, 1 L/min). The average acquisition time was 40 min, including anesthesia induction. A pressure sensor was used to monitor the respiratory rate, and respiratory-gating was used to minimize motion artifacts.

T2-weighted images were used to evaluate the extent of the lesion. Regions of interest (ROIs) were outlined for volumetric analysis, avoiding the brain-skull interface and ventricles, throughout the entire extension of the brain (excluding olfactory bulbs and cerebellum). Lesion was defined as cortical/subcortical areas with hyper-intense signal (cytotoxic edema) and/or signal void areas (tissue cavity) from T2-weighted images. Volumes of the lesion and of the ipsi- and contralateral hemispheres were measured using Aedes (http://aedes.uef.fi), an in-house written MatLab program (MathWorks, Natick, MA). The lesion volume and the volumes of ipsilateral and contralateral healthy hemispheres were calculated from 80 consecutive slices in the coronal plane, and adjusted in the sagittal plane (66 slices), and in the axial plane (99 slices).

Quantification of brain infarct volume and tissue loss

Measured volumes from MRI analysis were used to quantify the brain infarct volume and the lesion-related tissue loss, as previously described (22). The relative percentage of infarct volume was calculated using the following formula: Infarct volume = (volume of contralateral hemisphere – (volume of ipsilateral hemisphere – measured lesion volume))/volume of contralateral hemisphere. Tissue Loss was determined with the following formula: Tissue loss = (volume of ipsilateral hemisphere – volume of contralateral hemisphere)/volume of contralateral hemisphere.

Analysis was performed blinded to the study groups. The infarct volume was measured from 22 TBI mice from the following experimental groups: wild type (WT)–CCI, n = 13; and K14-VEGFR3-Ig (K14)–CCI, n = 9.

Preparation of Leukocytes

Thirty days after TBI induction, mice were anesthetized with an overdose of Avertin (Sigma, St. Louis, MO, USA) then transcardially perfused with ice-cold heparinized saline. Brains were collected and placed on ice in calcium and magnesium-free Hanks Balanced salt solution (HBSS) with 25 mM HEPES (both from Sigma).

Based on the analysis of MRI, we defined a priori the mean extension of the lesion and of the perilesional areas for all the TBI mice. Brains were sliced using a 1 mm scored matrix (Zivic Instruments, Pittsburgh, PA, USA): 6 mm thick coronal cut encompassing the lesion area was split along the central sagittal axis into left injured and right uninjured sides. Cortical areas, enclosed between the rhinal and the sagittal sulci, and the corresponding hippocampi, were further isolated and placed in HBSS+HEPES. From the injured sides, penetrated cortical areas were visually identified (lesion area - Supplementary Figure 1) and carefully excised along the lesion ridge to pick only the perilesional cortex for the further purification of leukocytes.

Brain samples were minced with scissors and then incubated at 37 °C on a roller for 30 min in digest buffer containing 1.25 mg/mL Collagenase Type 4 (Worthington, Lakewood, NJ, USA) and 100 U/mL DNAseI (Sigma) in DMEM + GlutaMAX (Gibco Thermo Fisher Scientific, Waltham, MA, USA). Samples were filtered through a 100 µm cell strainer (Corning, Weisbaden, Germany), and centrifuged at 600 x g for 5 min. Myelin debris was removed using Debris Removal Solution (Miltenyi Biotech, Bergisch Gladbach, Germany) according to the manufacturer's protocol. Briefly, cells were resuspended in ice-cold D-PBS (Sigma) with Debris Removal Solution then overlaid with ice-cold PBS and centrifuged at 2500 x g for 10 min at 4 °C. Supernatant including myelin layer was carefully removed leaving the clear phase and the pellet. Samples were washed in cold D-

PBS, centrifuged at 600 x g for 10 min at 4 °C, and the recovered pellets were resuspended in 200 µL of wash buffer for flow cytometry staining.

Spleens were isolated and collected in ice-cold HBSS+HEPES and processed by crushing through a 70 µm cell strainer (Corning), washed with ice-cold HBSS+HEPES, centrifuged 500 x g for 5 min before red blood cells were lysed in 1X PharmLyse (BD Biosciences, San Jose, CA USA) for 8 min at room temperature (RT). Cells were washed with HBSS+HEPES, centrifuged as above, resuspended in RPMI-1640 (Sigma), and counted on a Bürker grid hemocytometer.

Flow Cytometry staining and analysis

Approximately 500 000 spleen cells and the total cells isolated from the brain were washed with PBS, and centrifuged at 400 x g for 5 min. The supernatant was removed, and then Zombie NIR fixable viability dye (1:1000 BioLegend, San Diego, CA, USA) was added for 15 min at RT. Without washing, CD16/32 FcR block (5 µg/ml, BD Biosciences) was added followed by an antibody mix containing TCRβ PE-Cy7 (1:100 clone H57-597), CD44 PE (1:300 clone IM7) (both BioLegend), CD4 FITC (1:500, clone RM4-5), CD8 PerCP eFluor710 (1:300, clone 53-6.7) (both eBioscience Thermo Fisher Scientific, Waltham, MA, USA), and CD69 APC (1:20, clone H1.2F3, Miltenyi Biotech).

All antibodies were used at titers determined empirically under experimental conditions. Cells were incubated for 30 min at 4 °C. Afterwards, samples were washed twice in HBSS with 1 % FBS and then run on FACSAriaIII (BD Biosciences) equipped with 488 and 633 nm lasers with standard configuration. Brain samples were run completely and 50 000 live events were collected for spleen samples. Compensations were made using OneComp Beads for antibody fluorescence (eBioscience Thermo Fisher Scientific) and ArC amine reactive beads for viability dye (Molecular Probes, Eugene, Oregon, USA). Fluorescent Minus One (FMO) controls were made to ensure gating. These control samples contained all antibodies except one to display fluorescent spreading error of compensated data in each channel (23). Data were analyzed using FCSExpress v5 (Denovo Software, Los Angeles, CA, USA) and FlowJo v10.4 (Treestar, Portland, OR, USA). The gating strategy used for the flow cytometry analysis of brain-isolated immune cells is reported in Figure 1.

CD3 immunohistochemical staining

Three mice per genotype were injured and sacrificed 30 days after TBI for the immunohistochemical (IHC) localization of T lymphocytes in the brain. Briefly, animals were transcardially perfused with ice-cold PBS followed by 4 % PFA. Brains were dissected and post-

fixed in 4 % PFA by immersion for 24 h at 4 °C. Thereafter, specimens were cryoprotected by incubation in 20 % glycerol (in 0.02 M potassium phosphate-buffered saline (KPBS), pH 7.4) for 48 h, frozen in N-pentane (3 min at -60 °C), and stored at -70 °C until sectioning. Frozen coronal sections were cut (1-in-6 series, 25 µm thick) with a sliding microtome, and sections were collected in tissue-collecting solution (30 % ethylene glycol, 25 % glycerol in 0.05 M PB) and stored at -20 °C until further processing. Three sections per brain (approx. 700 µm apart, encompassing the antero-posterior extension of the lesion) were used for IHC detection of CD3+ infiltrating T lymphocytes. Floating sections were washed in three changes of 1X phosphate-buffered saline, pH 7.4 (PBS) before being incubated for 1 h at RT in blocking solution (2 % normal goat serum, 1 % bovine serum albumin (BSA) 0.1 % Triton X-100 and 0.05 % Tween20 in PBS). Sections were incubated with rat anti-mouse CD3ε (clone 17A2, eBioscience Thermo Fisher Scientific) diluted 1:500 in PBS with 1 % BSA and 0.05 % Triton X-100 overnight at 4 °C. After washing in three changes of PBS, sections were incubated with Alexa Fluor® 647-conjugated goat anti-rat secondary antibody (Thermo Fisher Scientific) diluted 1:500 in PBS with 1 % BSA and 0.05 % Triton X-100 for 1 h at RT. Finally, the sections were washed in PBS (3x) and, after 10 min with 1X phosphate buffer pH 7.4, mounted on Superfrost Plus slides (Thermo Scientific) with Vectashield (Vector Laboratories, Burlingame, CA, USA) and cover slipped. Panoramic photomicrographs of the stained sections were captured using 20X objective with a fluorescence microscope (Zeiss Observer.Z1), and high-resolution Z-stack images were captured using 20X objective with a confocal microscope (Zeiss LSM710). ZEN 2012 software (Carl Zeiss GmbH) was used for image processing. Due to the technical limitations related to CD3ε immunostaining, we used the stained sections exclusively to define the areas of T cell infiltration and not for its quantification.

Statistical analysis

Data exclusion criteria – We conducted 9 independent experiments, where a total of n = 16 “WT CCI”; n = 12 “WT naïve”; n = 13 “K14 CCI” and n = 10 “K14 naïve” mice have been analyzed.

Before statistical analysis, brain-derived samples were checked for their quality, based on total T cell recovery. Each sample has been considered independently, and we evaluated the T cell viability and the total number of T cells recovered. Brain samples where T cell viability was below 75 % or the total number of live T cells was below 100 counts were a priori excluded from the analyses. Samples derived from one animal (K14 CCI) were excluded due to sample handling problems.

Considering two genotypes (WT and K14) and three experimental conditions (T cells infiltrating the brain tissue ipsilateral to the lesion – “ipsi”; T cells infiltrating the tissue contralateral to the

lesion – “contra”, and T cells from naïve brain tissue – “naïve”), a total of n = 12 “WT ipsi”; n= 7 “WT contra”; n = 5 “WT naïve”; and n = 10 “K14 ipsi”; n = 7 “K14 contra”; n = 9 “K14 naïve” were eventually used for statistical analyses.

T cell viability > 90 % was used for the quality requirement of spleen samples. Moreover, we excluded samples presenting more than 50 % of necrotic tissue (defined as dark red non-perfused area in the spleen). Considering two genotypes (WT and K14) and two experimental conditions (CCI and naïve), a total of n = 13 “WT CCI”; n= 12 “WT naïve”; and n = 11 “K14 CCI”, n = 9 “K14 naïve” were used for subsequent statistical analyses.

Statistical analysis of brain-related data – Due to the small amount of T lymphocytes in naïve brains, brain samples were fully acquired on the flow cytometer, and for each population we analyzed both the absolute counts and the percentage referred to the respective parent population. Statistic models were applied considering the nature of our data (counts or percentages) and the experimental groups analyzed. A binomial negative regression was applied to assess statistical differences in the counts of total T cells, of CD4+, and of CD8+ cells between the two genotypes or within the same genotype between independent data. The binomial negative regression took into account both genotype and treatment, and their interaction. Because, within the same genotype, data from ipsi and contralateral brain sides are dependent, a linear mixed model was carried out to evaluate the differences in the total number of T lymphocytes, CD4+, and CD8+ T cells between “WT ipsi” vs. “WT contra” or “K14 ipsi” vs. “K14 contra”. As the data were not normally distributed (Shapiro-Wilk test p-value < 0.05), statistical differences between independent data in CD4+ and CD8+ T cell populations (expressed as percentage of T cells), as well as in the percentages of respective subpopulations expressing CD44 and/or CD69 antigens, were analyzed performing the Kruskal Wallis test. Dependent data within the same genotype (ipsi vs. contra) were analyzed performing the paired samples Wilcoxon signed ranked test. In all tests, Bonferroni correction was used to adjust p-values in multiple comparison.

Statistical analysis of data from spleen – All data from spleen are expressed as percentage of the parent population. After establishing the normal distribution of the data (as well as skewness and kurtosis by D’Agostino K-squared test), statistical differences were analyzed performing the Kruskal Wallis test or the paired samples Wilcoxon signed ranked test, depending on the nature of the data (independent or dependent), followed by Bonferroni adjustment.

Statistical analysis of MRI data – The differences in infarct volume and in tissue loss were analyzed performing the Kruskal Wallis test. Correlation between TBI-related tissue loss and infarct volume

was analyzed by Pearson linear regression, after checking for normality distribution of data as described before.

Statistical analyses were performed using R v3.5.3 software/computing environment (The R foundation for statistical computing). All software packages (MASS, psych, agricolae, multcomp and lme4) (24-28) were taken from the Comprehensive R Archive Network mirror sites (CRAN; http://CRAN.R-project.org/package=boot). Significance was accepted at the level of $p < 0.05$.

Results

T cells preferably infiltrate the cortical areas ipsilateral to the lesion

The presence of infiltrating T lymphocytes in the parenchyma is a signature of brain lesion. As first step in characterizing T cell infiltration at a chronic time point after TBI, we analyzed T cell presence in the area of injury and in other brain areas not directly affected by the penetrating injury. For this purpose, we stained the brains of both WT and K14-VEGFR3-Ig mice for the presence of the co-receptor CD3 (a specific marker of T lymphocytes), sacrificed 30 days post-injury (dpi). As expected, T cells are massively present within the boundaries of the injured area (Figure 2A, B). CD3+ cells are also spread throughout the cortical parenchyma, both in proximity of the lesion core (Figure 2C), and in more distal areas ipsilateral to the lesion, along the cortical layers. A strong immunostaining was also found along the corpus callosum (Figure 2D) while a minor presence of T cells was observed in the striatum, in the hippocampus and in the thalamus ipsilateral to the lesion (Figure 2A). Dim CD3+ signal was present in the contralateral hemisphere, indistinguishable from non-injured mice (data not shown). There was no difference in T cell distribution between WT and K14-VEGFR3-Ig mice. Both unevenly scattered cells (Figure 2E) and T cell clusters (Figure 2C, D) were observed within the parenchyma, suggesting the presence of clonal expansion of activated T cells.

As a next step, we decided to further characterize the populations of infiltrating T lymphocytes using flow cytometry, focusing on the neo-cortical areas (cortices and hippocampi), excluding the lesion area, which is characterized by a dysregulated entrance of immune cells (29).

Thirty days after brain trauma induction in WT and littermate K14-VEGFR3-Ig mice, leukocytes were purified separately from the perilesional and the contralateral cortices (or from the cortex of both WT and K14-VEGFR3-Ig naïve mice). T cells were identified by staining for T cell receptor (TCRβ) and the presence of the co-receptors CD4 and CD8. The acquired count of live T cells in the different experimental conditions is reported in Figure 3. A significant ~10-fold increase in

infiltrating T cells was found in both WT (median = 1449; Q3-Q1 = 1692), and K14-VEGFR3-Ig (median = 1741; Q3-Q1 = 892) mouse brains in the perilesional cortices, compared to corresponding naïve non-injured mice (WT naïve: median = 242; Q3-Q1 = 105; K14 naïve: median = 197; Q3-Q1 = 66; for statistical analysis, see Figure 3A). The number of TCRβ+ cells in the cortices contralateral to the lesion, instead, was not different from naïve brains (WT contra: median = 201; Q3-Q1 = 84; K14 naïve: median = 239; Q3-Q1 = 155; for statistical analysis, see Figure 3A). No genotype-related differences were observed (Figure 3A).

Perilesional infiltrating T cells have a predominant CD8+ phenotype and the lack of a functional lymphatic system depresses the T cell CD4-mediated response

We next analyzed the CD4:CD8 ratio within the infiltrating T cells (Figure 3B), and found a prevalence of CD8+ T cells in all the experimental conditions, regardless the presence of brain injury. However, limited to the perilesional cortex of K14-VEGFR3-Ig mice, we detected a significant skew of the CD4:CD8 ratio towards CD8+ cells (CD4:CD8 ratio K14 ipsi = 0.097±0.053; WT ipsi = 0.350±0.197; ChiSq: 8.836, mean ranks: 5.50/13.27, p = 8e-04 Bonferroni adjusted), while the ratio in the contralateral cortex did not differ between the two genotypes (CD4:CD8 ratio K14 contra = 0.221±0.247; WT contra = 0.456±0.212; ChiSq: 2.469, mean ranks: 5.43/8.83, p = 0.120 Bonferroni adjusted). To better understand how the lack of mLVs affects the T cell-mediated neuro-immune response, we analyzed both the absolute numbers of CD4 and CD8 subpopulations and their relative frequency. Data analysis shows a reduction of the total number of CD4+ T cells infiltrating the perilesional cortices of K14-VEGFR3-Ig (median = 106; Q3-Q1 = 156), compared to WT mice (median = 245; Q3-Q1 = 218; ex. coef.: -0.82, p = 0.033 K14 ipsi vs. WT ipsi, Bonferroni adjusted) (Figure 4A). No differences were observed in the absolute number of infiltrating CD8+ T cells between the genotypes (Figure 4B). Despite no differences in absolute numbers of both CD4 and CD8 populations in the contralateral cortices of injured WT and K14-VEGFR3-Ig mice, we found a significant reduction in the frequency of CD4+ T cells in transgenic mice (K14 contra = 12.04±8.47 %; WT contra = 23.59±9.52 % of T cells; ChiSq: 3.931, mean ranks: 5.29/9.71, p = 0.042 Bonferroni adjusted), and in the relative frequency of CD8+ T cells (Figure 4C, D). These data are in line with previous studies indicating the importance of a correct antigen drainage to dcLNs for the promotion of the CD4-mediated neuro-immune response (15, 17).

The presence of live CD8+ T cells in the perilesional cortices (together with the presence of T cell clusters, as shown by IHC staining) suggests a cytotoxic role for the infiltrating T cells at this time point. However, different subpopulations of CD8+ and CD4+ T cells exist, with specific and

opposing functions. As a secondary outcome, we characterized both the CD8+ and CD4+ subpopulations for the surface expression of the antigens CD44 (a memory and activation marker)(30, 31) and CD69 (an activation and tissue retention marker) (32). In the perilesional cortex of both WT and K14-VEGFR3-Ig mice, CD8+ T cells had a predominant $CD44^{hi}CD69+$ phenotype (69.78±22.85 % and 72.05±19.95 % of CD8+ T cells, in WT ipsi and K14 ipsi, respectively)(Figure 5A, B and Supplementary Table 2). The second most expressed CD8+ subpopulation (representing the 27.07±26.10 % in WT and the 25.24±18.85 % in K14-VEGFR3-Ig mice) had a $CD44^{hi}CD69-$ phenotype, characteristic of effector memory T cells (33). The presence of other CD8+ subpopulations among perilesional infiltrating T cells was negligible. No genotype related difference was found.

Among CD4+ perilesional infiltrating T cells, we found a similar frequency of subpopulations expressing CD44 and CD69 antigens, with a slight prevalence of $CD44^{hi}CD69+$ over $CD44^{hi}CD69-$ T lymphocytes (Figure 5C, D and Supplementary Table 2), in both genotypes. The overall frequency distribution of the different subpopulations was identical between the two genotypes.

Cortical lesion is similar in K14-VEGFR3-Ig mice and in their WT littermate

Analyses of MRI images acquired 21 days after TBI induction revealed a T2 intensity increase in the ipsilateral hemisphere. The increase of T2 intensity was observed in the parietal-temporal cortices, mainly involving the somatosensory and the visual cortices (Figure 6A), expanding in a few cases to the underlying hippocampus. No significant change of T2 intensity was found between the two genotypes. In the WT CCI group the infarct volume was 4.67±1.35 %, and 4.09±2.00 % in the K14-VEGFR3-Ig injured animals (ChiSq: 0.579, mean ranks: 8.71/10.75, $p = 0.463$)(Figure 6B). Relative tissue loss was 2.64±1.27 % in WT CCI mice and 2.00±1.26 % in K14 CCI mice (ChiSq: 1.400, mean ranks: 8.00/11.17, $p = 0.248$)(Figure 6C). Correlation between infarct volume and relative tissue loss was compared in transformed data with linear regression analysis. When considering the individual values independent of the genotype, the infarct volume values significantly correlated with the values of relative tissue loss ($r = 0.61$; $p = 0.005$)(Figure 6D). Similarly, the infarct volume in the K14 CCI group correlated with the mean value of the brain swelling ($r = 0.74$; $p = 0.051$), while no correlation was found in the WT CCI mice ($r = 0.50$; $p = 0.101$).

K14-VEGFR3-Ig mice present a peripheral lymphopenia, which is exacerbated after TBI

Alterations of systemic immunity are frequent in TBI patients. We analyzed the levels and the frequency of different T cell subpopulations in the spleen of WT and K14-VEGFR3-Ig mice, one

month after TBI induction. As previously described (34), K14-VEGFR3-Ig mice show a moderate lymphopenia compared to littermate WT mice (percentage of T cells over live cells in WT naïve: 37.26±7.67 %; vs. K14 naïve: 19.69±4.96 %; ChiSq: 14.746, mean ranks: 5.00/15.50, p = 1e-04 Bonferroni adjusted)(Figure 7A). Contrary to what was observed in the brain, the systemic lymphopenia in K14-VEGFR3-Ig genotype corresponds to a relative frequency reduction in peripheral CD8+ T cells (K14 naïve = 25.75±3.61 %; WT naïve = 42.70±4.17 % of T cells; ChiSq: 14.727, mean ranks: 5.00/15.50, p = 1e-04 Bonferroni adjusted)(Figure 7B). In K14-VEGFR3-Ig mice, but not in WT mice, we found a significant reduction in the total T cells frequency after TBI (WT CCI: 33.68±6.99 %; K14 CCI: 14.23±2.87 % of live cells; ChiSq: 7.695, mean ranks: 7.18/14.55, p = 0.003 K14 CCI vs. K14 naïve, Bonferroni adjusted)(Figure 7A), confirming that K14-VEGFR3-Ig present an impaired immune response, which relates to the alterations in the lymphatic system. Analysis of the activation markers show a different expression in both CD4 + and CD8+ subpopulations between WT and K14-VEGFR3-Ig mice, which is trauma independent. Both K14 naïve and K14 CCI mice, indeed, showed an increased frequency of memory T cells (CD4+CD44^{hi}CD69+, CD4+CD44^{hi}CD69- and CD8+CD44^{hi}CD69+, CD8+CD44^{hi}CD69-; for statistical analysis, see Supplementary Table 3)(Figure 7C, D).

Discussion

The results of this study show the effects of the deficiency of functional CNS lymphatic system on the chronic T cell-mediated immune response following TBI.

Mounting evidence implicate a modulation of a T lymphocyte-mediated immune response as a result of TBI. In the CNS, T cell infiltration after trauma has been observed in human (35-37) and animal models of brain injuries, both at acute and chronic time points (6, 8-10, 38): however, a characterization of this adaptive neuro-immune response is so far missing.

Our data confirm that the early chronic phases after TBI are characterized by a sustained brain infiltration of T lymphocytes (6, 8, 10), which is restricted to the cortical areas surrounding the lesion. In WT (C57Bl/6JOla) injured mice, infiltrating T cells have predominantly a cytotoxic phenotype (expressing the T cell co-receptor CD8), with approximately a 25:75 CD4/CD8 ratio. In the K14-VEGFR3-Ig transgenic mice deficient in functional mLVs (responsible for the drainage of CSF into the dcLNs, where T cells are specifically activated), the immune response after TBI is characterized by a downregulation of CD4+ T cells, with cytotoxic CD8+ T lymphocytes representing more than 90 % of total infiltrating T lymphocytes. We attribute this effect to the

impairment of the specific neuro-immune circuit, involving mLVs and dcLNs, responsible for the specialized immune response observed in the CNS (15-17).

Moreover, our data also originally indicate that systemic- and neuro-immune responses after brain injury are independently regulated, resulting in a strong adaptive immune response in the brain, even in the absence of a systemic immune reaction. Specifically, our findings suggest that: 1) immune response in the brain at early chronic time points after TBI is principally mediated by cytotoxic CD8+ T cells; 2) the circuit CNS lymphatic system is essential to modulate the specific neuro-immune response; 3) in the chronic phase after TBI, the response of peripheral T lymphocytes does not correlate with the neuroimmulogical state of the brain.

Brain trauma results in two phases of tissue injury. The primary injury, a direct result of the mechanical impact to the brain tissue, is characterized by neuronal and glial cell death, axonal injury, and disruption of the blood–brain barrier (BBB) possibly associated with subarachnoid hemorrhage. In a cascade of events, the activation of an innate immune response (including neuro-inflammation and infiltration of neutrophils and macrophages), and the release of excitotoxic agents contribute to early secondary injuries, characterized by cytotoxic edema (39). During this acute phase, a massive and dysregulated brain-infiltration of T cells has been reported (40, 41). A secondary tissue damage, resulting in a diffuse and long-lasting injury, usually develops after months/years from the primary injury. This is characterized by additional neurodegeneration developing independently from the mechanical trauma, and by the formation of a fibrotic scar tissue in the injured area (42). Recent data have reported that, at chronic time points post-TBI, a second wave of T cell infiltrates the brain (8, 10), suggesting the development of an adaptive immune response, which can contribute to the development of the secondary injuries. It is, therefore, important to understand the role of the adaptive immune response in the contest of the TBI pathology: in this view, aim of the present work is to characterize which T cell subpopulations are present within the brain parenchyma during the second wave of immune response, and to define their activation state.

Mounting of an adaptive immune reaction require the specific activation of T cell within the lymph nodes. The deep and superficial cervical lymph nodes (dcLNs and scLNs, respectively) represent the regional lymph nodes draining the CNS antigens (16) and play an active role in defining the type and the magnitude of the neuro-immune response (15, 17, 43, 44). Experimental evidence has suggested that in the dcLNs a specific T-helper (Th) immune response is elicited against brain-derived antigens (17), which is polarized towards Th2 and regulatory (Treg) CD4+ T cells (15, 45). This specific response, sustaining a microenvironment within the brain that inhibits the pro-

inflammatory and cytotoxic activity, concurs to the unconventional regional immune regulation of the CNS. Meningeal lymphatics are the initial collector lymphatic vessels, involved in the drainage of solutes from the interstitial and cerebro-spinal fluids mainly to the dcLNs (13, 14): mLVs represent, therefore, an integrated component in the immune response to brain insults (13). It is conceivable to hypothesize that a functional damage to the mLVs can affect the type of evoked neuro-immune response. To address this hypothesis, we used a transgenic mouse model of congenital lymphedema caused by an impaired lymphangiogenesis in several organs, including the CNS (18). K14-VEGFR3-Ig mice express soluble VEGFR-3-Ig, resulting in defective growth of mLVs and in sclerotic dcLNs, while scLNs do not seem to be affected (14, 46). In these mice, the peripheral immune response is compromised with an impaired humoral immunity and a delayed but robust T cell response to immunization (34).

Our data, showing a higher CD4/CD8 T cell ratio in the spleen of K14-VEGFR3-Ig mice compared to WT littermates, confirmed the reported evidence of alterations in the immune system in the absence of proper functional lymphatics. On the other hand, within the brain of transgenic mice we observed a concurrent marked decrease in the frequency of infiltrating CD4+ T cells and a polarization towards a CD8+ cytotoxic neuro-immune response. We suggest that in K14-VEGFR3-Ig mice the activation of the Th2/Treg-mediated immune response, within the dcLNs, is bypassed. As a result, there is a shift of infiltrating T lymphocytes towards cytotoxic CD8+ cells that can end up in an organ-specific autoimmune response, which sustains the secondary neurodegeneration observed in TBI patients.

However, the presence of infiltrating CD8+ T lymphocytes per se does not indicate that they are effectively mounting a cytotoxic response: lymph node-primed CD8+ T cells need to be activated at the site of inflammation in order to carry out their cytotoxic activity. It is therefore important to characterize in addition the activation state of the T cells that infiltrate the perilesional cortex. In our experimental conditions, we have found that, independently from the analyzed genotype, infiltrating T lymphocyte are prevalently CD8+ with a $CD44^{hi}CD69+$ phenotype.

CD69 is an early marker of T cell activation (32), suggesting that the CD8+ T lymphocytes found in the perilesional areas could be selectively activated. As a confirmation of this, on the contralateral side we found a significant increase of $CD8+CD44^{hi}$ T cells with a negative CD69 phenotype (data not shown). This indicates that the immune response is activated only in the site of lesion, where neuro-inflammation is expected. Another subpopulation of T lymphocytes expressing CD69 are the mature resident memory T cells, which are generated, and persist, in the tissue at the site of a primary infection. These cells constitutively express CD69, limiting their exit from the lesion area

and the return to the blood and lymphatics (33). Resident memory T cells provide a first line of adaptive cellular defense. In the case of TBI, they may represent the population of T cells designated to defend the non-injured brain from possible infective agents penetrating through the lesion. Further studies are required to comprehensively characterize the phenotype of the CD8+ T cell population infiltrating the brain, their ability to undergo clonal expansion and to release effector cytokines (e.g. IFNγ), and to determine the antigen specificity.

In our experimental conditions, within the CD4+ population of T cells infiltrating the perilesional cortex, we found a slight prevalence of $CD44^{hi}CD69+$, suggesting that also the resident memory T helper cells are activated in support of the CD8+ immune response.

A compelling idea is that the adaptive immune system underpins and sustains tissue damage after brain injury: CD8+ T lymphocytes, supported by CD4+ Th1 cells, worsen the damage by cytotoxic action, whereas CD4+ Th2 and Treg cells may exert anti-inflammatory, neuroprotective action (47). Our data, showing a pronounced CD8+ T cell infiltration associated with a marked reduction of CD4+ T cells and a negligible presence of Treg (data not shown), infer a worsening effect of the chronic adaptive immune response on brain damage. However, the analysis of lesion size on MRI scans, acquired 7 days before sample collection for flow cytometry, does not show any significant difference between the two different genotypes. There are a few possibilities to explain the lack of increasing damage in the presence of a higher frequency of infiltrating CD8+ T cells, as observed in K14-VEGFR3-Ig mice. First, we have identified the lesion size as the hyper-intense signal in the cortical area observed in the T2 weighted images. A hyper-intense signal in this MR sequence results from edema-related water accumulation, affecting our analysis of the brain lesion. One possibility is that the increased infiltration of cytotoxic CD8+ T cells in K14-VEGFR3-Ig mice does not directly affect the formation/clearance of the intraparenchymal edema. Another hypothesis can be found in the kinetics of the secondary neurodegeneration. Although triggered by cytotoxic T cells, secondary neurodegeneration may appear at a later time point than the one analyzed in this study. Finally, an explanation could be reckoned on CD4 populations: namely the Th1, Th2 or Th17 populations. Interestingly, we found a direct correlation between the frequency of CD4+ T cells and the percentage of tissue loss in K14-VEGFR3-Ig mice but not in WT littermates (Supplementary Figure 2), suggesting the presence of a distinct population of infiltrating CD4+ T lymphocytes in the perilesional cortices of K14-VEGFR3-Ig mice compared to WT littermates. However, the panel of antibodies used for the T cell characterization does not allow us to distinguish between CD4+ T helper populations; therefore, we cannot speculate further on the role of these cells in the lesion formation. Further studies are needed to understand the role of cytotoxic CD8+ and of associated

CD4 T-helper lymphocytes on anatomical and functional brain damage after TBI, exploring their effects at different chronic time points.

From the clinical point-of-view, patients with severe TBI show high susceptibility to systemic infections, which are associated with declining neurological outcome and increased mortality. TBI itself is an important risk factor for infection complication. While TBI is associated with an immediate systemic inflammatory response (39), severe brain injury leads also to a delayed secondary immunodeficiency (CNS injury-induced immunodepression, CIDS), characterized by a reduced number of circulating T lymphocytes (48, 49). In patients with severe TBI, lymphopenia is observed in peripheral blood soon after injury, due to a reduction of both CD4+ (49) and CD8+ (50) circulating T cells, lasting up to several weeks (48). Therefore, we analyzed the levels of circulating T lymphocyte in our model to analyze if these reflect the neuroimmunological state of the brain, and if the acute lymphopenia is protracted to the chronic time point analyzed in this study.

It has been proposed that CNS injuries could dampen cell-mediated immune responses via three pathways: the hypothalamo–pituitary–adrenal (HPA) axis, the sympathetic nervous system, or the parasympathetic system (48). Another proposed hypothesis is the compartmental shift of T lymphocytes in the CNS (49). Based on the analysis of brain and spleen lymphocyte levels in WT mice in our experimental conditions, we can exclude the compartmental shift hypothesis. WT mice showed a strong infiltration of T lymphocytes in the brain perilesional areas. If this would be the result of a compartmentalization of T cells, we should expect to observe a drastic reduction of their level in the spleen. Nevertheless, we found no differences in T cell levels (both CD4+ and CD8+) in the spleen between naïve and CCI animals, in either genotype. At the same time, a drastic reduction in CD8+ frequency in the spleen, independently from brain trauma, was observed in this study in K14-VEGFR3-Ig compared to WT mice. These data confirm a previous report, describing a constitutive systemic lymphopenia in K14-VEGFR3-Ig mice (34), which, as we here demonstrate, does not reflect the levels of T cell-mediated neuro-immune response.

It is out of the scope of this study to determine the mechanisms underlying the observed lymphopenia in TBI. However, analysis of our data excludes a correlation between the extent of brain infiltration and the level of T cells in the periphery (data not shown), suggesting the possibility of a severe neuro-immune reaction even in the presence of a systemic congenital lymphopenia (as in K14-VEGFR3-Ig mice). This is an interesting observation with potential clinical implications, because patients with CIDS could at the same time present a sustained adaptive immune response localized in the brain. In this specific case, patients would benefit from a

targeted immunomodulatory therapy in the brain, not impinging on the already compromised systemic immunity.

Our data suggest that, in the presence of chronic neuro-inflammation (as it is the case after TBI (51, 52)), the neuro- and systemic immune responses are independent. This is apparently in contrast with previously published data (6), where Authors found a substantial correlation between the levels of different T cell populations in the brain and in the blood after TBI. However, in their work Braun and colleagues focus their analyses on an early time point after TBI (3 dpi), which is characterized by an ongoing brain hemorrhage, and analyzed a portion of the injured brain which includes the lesion itself. In our work, we analyzed an early chronic time point (30 dpi), where we could not find visible sign of hematoma (both in MRI and by visual inspection of the brain tissue at the time of euthanasia). Moreover, we excised the lesion area before collecting the brain tissue for lymphocyte isolation. Our samples, therefore, includes only the T cells that were able to bypass the scar tissue and infiltrate in the perilesional brain areas, possibly contributing to the secondary injuries in TBI pathology.

The role of T lymphocytes in the progression of brain damage following TBI is largely unknown. Empirical and experimental evidence indicate that seemingly similar types of trauma result in diverse clinical outcomes. Heterogeneity of recovery time and the extent of neurological dysfunction in TBI can only be partially explained by differences in the severity and location of brain injury (53). Our data support the role of the neuro-immune system as a key player in TBI pathophysiology and as a possible factor of heterogeneity in TBI outcome. The nature and kinetics of the immune responses can vary depending on brain injury location and severity, and in experimental TBI studies the exact kinetic of T lymphocyte infiltration depends on the different TBI models used. In our experimental conditions, we demonstrate that, at early chronic time points after brain injury, resident memory T cells are activated in the perilesional areas as part of an adaptive immune response. These data support the possibility of a targeted CD8-mediated immune response, which could contribute to the secondary delayed phase of tissue damage. However, transient autoimmune reactions have been reported in different models of brain injuries, with a proposed beneficial activity (54, 55), and studies aimed to downregulate the adaptive immune response after TBI did not improve the neurological outcome (56). On the other hand, it is important to note that these studies were focused on manipulating the early wave of T cell infiltration after TBI. No other studies, to the best of our knowledge, have specifically targeted the subsequent adaptive immune response, which is a novel characterization in our study. Understanding the processes underlying

and sustaining the adaptive neuro-immune response after brain injury, therefore, is important to elucidate how secondary brain lesions develop, as well as defining potential therapeutic targets.

Conclusions

To our knowledge, our study is the first aimed at investigating the phenotype of infiltrating T lymphocytes in the brain after TBI, clearly showing an activation of the immune adaptive arm in response to an earlier lesion. Our findings also support the importance of meningeal lymphatic vessels and of afferent deep cervical lymph nodes in maintaining brain immuno tolerance. We propose that systemic- and neuro-immunity are distinct processes driven by different secondary lymphoid organs. Modulation of the neuro-immune response by acting on the CNS-mLVs-dcLNs pathway could therefore eventually constitute a therapeutic strategy for TBI patients.

Acknowledgments

This study has been supported by the Academy of Finland (Academy of Finland research Fellowship #309479/2017 – FMN), by the Jane and Aatos Erkko Foundation (JK and prof. Kari Alitalo’s group) and by European Research Council (ERC) under the European Union's Horizon 2020 research and innovation programme under grant agreement #743155 (KA).

Authors would like to thank prof. Kari Alitalo for his critical review on data and manuscript, and for the support provided to the study.

For his help with MRI sequences, we would like to thank Mikko Kettunen from Biomedical Imaging Unit, National Bio-NMR facility, A.I.Virtanen Institute for Molecular Sciences, University of Eastern Finland. Finally, we would like also to Flavia Scoyni and Bengisan Dvirick for their contribution in performing experiments.

Author Contributions

FMN originally conceived the study; SW and FMN elaborated the study design; SW, MHK and FMN performed experiments; MV analyzed the data; BG and FMN performed the statistical analysis; SW, MV, BG and FMN drafted a significant portion of the manuscript and figures. SA wrote sections of the manuscript. JK supported the study and provided critical review to the

manuscript. All authors contributed to manuscript revision, read, and approved the submitted version.

Conflict of Interest Statement

None of the authors has any conflict of interest to disclose. The authors confirm that have read the Journal's position on issues involved in ethical publication and affirm that this report is consistent with those guidelines.

Data Availability

The raw data supporting the conclusions of this manuscript will be made available by the corresponding author, upon reasonable request, to any qualified researcher.

Legend to Figures

Figure 1. ***Gating strategy.*** Flow cytometry analysis scheme showing how isolated immune cells in the brain were gated for live cell analysis. Mononuclear cells were selected based on light scattering properties (A) and doublets were removed (B, C). Among gated events, live cells were defined as negative for fixable viability dye (FVD) staining (D), and T cells were identified as positive for TCRβ (E). TCRβ+ lymphocyte subsets were characterized by the expression of CD4 and CD8 cell surface markers (F). Gating was determined using FMOs (see Methods section).

Figure 2. ***Localization of CD3+ T cells in the perilesional cortices.*** Representative images of brain sections from WT **(A)** and K14-VEGFR3-Ig **(B)** mice 30 dpi, stained for anti-CD3ε (T lymphocytes; red). The lesion edges in each section are marked with a segmented yellow line. T cells are present within the lesion (star in A and B), in the perilesional cortex (box in A and panel C) and in the corpus callosum (box in A and panel D). CD3+ cells were also observed in the striatum (arrow in A and B) and in the thalamus (arrow head in A). Both scattered cells and clusters of T cells were found within the parenchyma (C and E, respectively). Panels **(C)** and **(D)** represent a magnification of the areas depicted within the white boxes in A. Panel **(E)** represents a magnification of the area depicted within the white box in B. (A and B, scale bar = 500 µm; C-E, scale bar = 20 µm.)

Figure 3. ***T cell brain infiltration is confined to the perilesional cortices, 30 dpi.*** Box plot representing the number of infiltrating T cells, defined by expression of TCRβ **(A)** and stacked bargram representing the percentage of CD4+ and CD8+ T cells **(B)** in the brain of WT and K14-VEGFR3-Ig mice, as analyzed in the perilesional and contralateral cortices (ipsi and contra, respectively), or in intact cortices from respective naïve mice. Independently from the genotype, a significant infiltration of TCRβ+ T cells was observed in the perilesional areas but not in the contralateral hemispheres (comparable to naïve non-injured brains). The majority of brain-infiltrating T cells presented a CD8 phenotype. In the K14-VEGFR3-Ig mice, there was a significant skew of CD4/CD8 ratio towards CD8+ T cells. Table **(C)** summarizes the results of the statistical analysis in T cell counts between the experimental groups. In (A) boxes represent the 25-75 % value range, including the median value, indicated with the line. Whiskers represent 1.5x standard deviation (SD). □ indicates the mean value. In the stacked bargram, data are presented as mean ± standard error of the mean (s.e.m.). A binomial negative regression or a linear mixed model was applied to assess statistical differences in the counts of total T cells. The Kruskal Wallis test or the paired samples Wilcoxon signed ranked test was used for the analysis of CD4 and CD8 frequency distribution. ¤$p < 0.05$ and ¤¤¤$p < 0.001$ vs. K14 ipsi. *$p < 0.05$ and ***$p<0.001$ vs. WT ipsi. In all tests, Bonferroni correction was used to adjust p-values in multiple comparisons.

Figure 4. ***The number of CD4+ but not of CD8+ T cells is reduced in the brain of K14-VEGFR3-Ig mice after TBI.*** Box plots representing the number and frequency of CD4+ T cells (**A** and **C**, respectively) and CD8+ T cells (**B** and **D**, respectively), in the brain of WT and K14-VEGFR3-Ig mice, as analyzed in the perilesional and contralateral cortices (ipsi and contra, respectively), or in intact cortices from naïve mice. A drastic reduction in the number of CD4+ T cells was found in K14-VEGFR3-Ig mice after injury. A binomial negative regression or a linear mixed model was applied to assess statistical differences in the counts of CD4+ and CD8+ T cells. The Kruskal Wallis test or the paired samples Wilcoxon signed ranked test was used for the analysis of frequency distribution. *$p < 0.05$; **$p < 0.01$ and ***$p < 0.001$ vs. WT ipsi. ¤$p < 0.05$; ¤¤$p < 0.01$ and ¤¤¤$p < 0.001$ vs. K14 ipsi. #$p < 0.05$ vs. WT contra. In all tests, Bonferroni correction was used to adjust p-values in multiple comparisons. For box plot explanation, refer to the legend of Figure 1.

Figure 5. ***Analysis of CD69 and CD44 T cell activation and memory markers in CD4+ and CD8+ subpopulations.*** Pseudocolor dot plots **(A)** and **(B)** represent gated subpopulations CD69 vs. CD44 of CD4+ and CD8+, respectively. Stacked bargrams in **(C)** and **(D)** show respectively the counts

and frequencies of CD8+ T cell subpopulations, as analyzed in the perilesional cortices of WT and K14-VEGFR3-Ig mice. No significant differences in CD8+ subpopulations were found between genotypes. In CD4+ subpopulation, instead, we observed a significant reduction in the counts of $CD44^{hi}CD69+$ and $CD44^{hi}CD69-$ subpopulations **(E)**, in K14-VEGFR3-Ig compared to WT mice. However, no differences were observed in the different subpopulation frequencies **(F)**. Data are presented as mean ± s.e.m. A binomial negative regression was applied to assess statistical differences in the counts of total T cells between WT ipsi and K14 ipsi. The Kruskal Wallis test was used for the analysis of frequency distribution. #$p < 0.05$; *$p < 0.05$ vs. WT ipsi.

Figure 6. ***TBI-induced lesions does not differ between the two genotypes, as inferred by the analysis of MRI at 21 dpi***. **(A)** Representative MR images of WT naïve, WT CCI, K14 naïve and K14 CCI brains. Perilesional cortices in WT CCI and K14 CCI brains are marked with stars. Box plots in **(B)** and **(C)** illustrate the genotype effect on the percentage of infarct volume and of tissue loss, respectively, over the volume of the hemisphere ipsilateral to the lesion. No significant differences were observed between K14-VEGFR3-Ig and WT mice. For the definitions of the infarct volume and of tissue loss see the main text. **(D)** When considering the infarct volume and the tissue loss independently from the genotype, we found a direct correlation between the two parameters. The Kruskal Wallis test was used for the analysis of infarct volume and of tissue loss between the two genotypes. CI: 95 % confidence interval. For box plot explanation, refer to the legend of Figure 1.

Figure 7. ***Peripheral immune response in the spleen.*** The percentages of T cells in the spleen of WT naïve and CCI mice and of K14 naïve and CCI mice are presented in the box plot in panel **(A)**. Stacked bargrams in **(B)** represent the relative percentages of CD4 and CD8 in T cell population, in WT and K14-VEGFR3-Ig mice. K14-VEGFR3-Ig mice present a drastic reduction of T cells compared to WT littermates, due to a decrease in CD8+ T cell frequency. **(C, D)** Representative pseudocolor dot plots and gating strategies for CD4+ and CD8+ T cell subpopulation analysis, respectively. Stacked bargrams in **(E)** and **(F)** show respectively the frequencies of CD4+ and CD8+ T cell subpopulations, as analyzed in WT and K14-VEGFR3-Ig mice. Significant differences in the frequencies of both CD4+ and CD8+ subpopulations have been observed. The Kruskal Wallis test or the paired samples Wilcoxon signed ranked test was used for the analysis of frequency distribution. ¤¤$p < 0.01$ and ¤¤¤$p < 0.001$ vs. K14 CCI. **$p < 0.01$ and ***$p < 0.001$ vs. WT naïve. In all tests, Bonferroni correction was used to adjust p-values in multiple comparison. For box plot and stacked bargram explanation, refer to the legend of Figure 1.

Bibliography

(1) Hale AC, Bohnert KM, Grekin R, Sripada RK. Traumatic Brain Injury in the General Population: Incidence, Mental Health Comorbidity, and Functional Impact. *J Nerv Ment Dis* (2019) **207**:38-42. doi: 10.1097/NMD.0000000000000915 [doi].

(2) Hyder AA, Wunderlich CA, Puvanachandra P, Gururaj G, Kobusingye OC. The impact of traumatic brain injuries: a global perspective. *NeuroRehabilitation* (2007) **22**:341-353.

(3) Langlois JA, Rutland-Brown W, Wald MM. The epidemiology and impact of traumatic brain injury: a brief overview. *J Head Trauma Rehabil* (2006) **21**:375-378. doi: 00001199-200609000-00001 [pii].

(4) Menon DK, Schwab K, Wright DW, Maas AI, Demographics and Clinical Assessment Working Group of the International and Interagency Initiative toward Common Data Elements for Research on Traumatic Brain Injury and Psychological Health. Position statement: definition of traumatic brain injury. *Arch Phys Med Rehabil* (2010) **91**:1637-1640. doi: 10.1016/j.apmr.2010.05.017 [doi].

(5) McIntosh TK, Smith DH, Meaney DF, Kotapka MJ, Gennarelli TA, Graham DI. Neuropathological sequelae of traumatic brain injury: relationship to neurochemical and biomechanical mechanisms. *Lab Invest* (1996) **74**:315-342.

(6) Braun M, Vaibhav K, Saad N, Fatima S, Brann DW, Vender JR, et al. Activation of Myeloid TLR4 Mediates T Lymphocyte Polarization after Traumatic Brain Injury. *J Immunol* (2017) **198**:3615-3626. doi: 10.4049/jimmunol.1601948 [doi].

(7) DeKosky ST, Kochanek PM, Clark RS, Ciallella JR, Dixon CE. Secondary Injury After Head Trauma: Subacute and Long-term Mechanisms. *Semin Clin Neuropsychiatry* (1998) **3**:176-185. doi: 00300176 [pii].

(8) Jin X, Ishii H, Bai Z, Itokazu T, Yamashita T. Temporal changes in cell marker expression and cellular infiltration in a controlled cortical impact model in adult male C57BL/6 mice. *PLoS One* (2012) **7**:e41892. doi: 10.1371/journal.pone.0041892 [doi].

(9) Bai R, Gao H, Han Z, Huang S, Ge X, Chen F, et al. Flow Cytometric Characterization of T Cell Subsets and Microglia After Repetitive Mild Traumatic Brain Injury in Rats. *Neurochem Res* (2017). doi: 10.1007/s11064-017-2310-0 [doi].

(10) Erturk A, Mentz S, Stout EE, Hedehus M, Dominguez SL, Neumaier L, et al. Interfering with the Chronic Immune Response Rescues Chronic Degeneration After Traumatic Brain Injury. *J Neurosci* (2016) **36**:9962-9975. doi: 10.1523/JNEUROSCI.1898-15.2016 [doi].

(11) Galea I, Bechmann I, Perry VH. What is immune privilege (not)?. *Trends Immunol* (2007) **28**:12-18. doi: S1471-4906(06)00326-7 [pii].

(12) Louveau A, Herz J, Alme MN, Salvador AF, Dong MQ, Viar KE, et al. CNS lymphatic drainage and neuroinflammation are regulated by meningeal lymphatic vasculature. *Nat Neurosci* (2018) **21**:1380-1391. doi: 10.1038/s41593-018-0227-9 [doi].

(13) Louveau A, Smirnov I, Keyes TJ, Eccles JD, Rouhani SJ, Peske JD, et al. Structural and functional features of central nervous system lymphatic vessels. *Nature* (2015) **523**:337-341. doi: 10.1038/nature14432 [doi].

(14) Aspelund A, Antila S, Proulx ST, Karlsen TV, Karaman S, Detmar M, et al. A dural lymphatic vascular system that drains brain interstitial fluid and macromolecules. *J Exp Med* (2015) **212**:991-999. doi: 10.1084/jem.20142290 [doi].

(15) Harling-Berg CJ, Park TJ, Knopf PM. Role of the cervical lymphatics in the Th2-type hierarchy of CNS immune regulation. *J Neuroimmunol* (1999) **101**:111-127. doi: S0165572899001307 [pii].

(16) Cserr HF, Harling-Berg CJ, Knopf PM. Drainage of brain extracellular fluid into blood and deep cervical lymph and its immunological significance. *Brain Pathol* (1992) **2**:269-276.

(17) Thomas DL, Kranz DM, Roy EJ. Experimental manipulations of afferent immune responses influence efferent immune responses to brain tumors. *Cancer Immunol Immunother* (2008) **57**:1323-1333. doi: 10.1007/s00262-008-0467-8 [doi].

(18) Makinen T, Jussila L, Veikkola T, Karpanen T, Kettunen MI, Pulkkanen KJ, et al. Inhibition of lymphangiogenesis with resulting lymphedema in transgenic mice expressing soluble VEGF receptor-3. *Nat Med* (2001) **7**:199-205. doi: 10.1038/84651 [doi].

(19) Hutchinson E, Avery A, Vandewoude S. Environmental enrichment for laboratory rodents. *ILAR J* (2005) **46**:148-161.

(20) Guedel AE. Stages of Anesthesia and re-classification of the signs of anesthesia. *Current Researches in Anesthesia & Analgesia:* (1927) **6**:157-162.

(21) Cole JT, Yarnell A, Kean WS, Gold E, Lewis B, Ren M, et al. Craniotomy: true sham for traumatic brain injury, or a sham of a sham?. *J Neurotrauma* (2011) **28**:359-369. doi: 10.1089/neu.2010.1427 [doi].

(22) Dhungana H, Rolova T, Savchenko E, Wojciechowski S, Savolainen K, Ruotsalainen AK, et al. Western-type diet modulates inflammatory responses and impairs functional outcome following permanent middle cerebral artery occlusion in aged mice expressing the human apolipoprotein E4 allele. *J Neuroinflammation* (2013) **10**:102-2094-10-102. doi: 10.1186/1742-2094-10-102 [doi].

(23) Roederer M. Compensation in flow cytometry. *Curr Protoc Cytom* (2002) **Chapter 1**:Unit 1.14. doi: 10.1002/0471142956.cy0114s22 [doi].

(24) Hothorn T, Bretz F, Westfall P. Simultaneous Inference in General Parametric Models. *Biometrical Journal* (2008) **50**:346-363.

(25) Bates D, M\achler M, Bolker B, Walker S. Fitting Linear Mixed-Effects Models Using lme4. *Journal of Statistical Software* (2015) **67**:1-48. doi: 10.18637/jss.v067.i01.

(26) Mendiburu Fd. agricolae: Statistical Procedures for Agricultural Research (2019).

(27) Revelle W. *psych: Procedures for Psychological, Psychometric, and Personality Research*. Evanston, Illinois: Northwestern University (2018).

(28) Venables WN, Ripley BD. *Modern Applied Statistics with S*. New York: Springer (2002).

(29) Fee D, Crumbaugh A, Jacques T, Herdrich B, Sewell D, Auerbach D, et al. Activated/effector CD4+ T cells exacerbate acute damage in the central nervous system following traumatic injury. *J Neuroimmunol* (2003) **136**:54-66. doi: S0165572803000080 [pii].

(30) Budd RC, Cerottini JC, Horvath C, Bron C, Pedrazzini T, Howe RC, et al. Distinction of virgin and memory T lymphocytes. Stable acquisition of the Pgp-1 glycoprotein concomitant with antigenic stimulation. *J Immunol* (1987) **138**:3120-3129.

(31) Ponta H, Sherman L, Herrlich PA. CD44: from adhesion molecules to signalling regulators. *Nat Rev Mol Cell Biol* (2003) **4**:33-45. doi: 10.1038/nrm1004 [doi].

(32) Ziegler SF, Ramsdell F, Alderson MR. The activation antigen CD69. *Stem Cells* (1994) **12**:456-465. doi: 10.1002/stem.5530120502 [doi].

(33) Topham DJ, Reilly EC. Tissue-Resident Memory CD8(+) T Cells: From Phenotype to Function. *Front Immunol* (2018) **9**:515. doi: 10.3389/fimmu.2018.00515 [doi].

(34) Thomas SN, Rutkowski JM, Pasquier M, Kuan EL, Alitalo K, Randolph GJ, et al. Impaired humoral immunity and tolerance in K14-VEGFR-3-Ig mice that lack dermal lymphatic drainage. *J Immunol* (2012) **189**:2181-2190. doi: 10.4049/jimmunol.1103545 [doi].

(35) Hausmann R, Kaiser A, Lang C, Bohnert M, Betz P. A quantitative immunohistochemical study on the time-dependent course of acute inflammatory cellular response to human brain injury. *Int J Legal Med* (1999) **112**:227-232.

(36) Holmin S, Soderlund J, Biberfeld P, Mathiesen T. Intracerebral inflammation after human brain contusion. *Neurosurgery* (1998) **42**:291-8; discussion 298-9. doi: 10.1097/00006123-199802000-00047 [doi].

(37) Dressler J, Hanisch U, Kuhlisch E, Geiger KD. Neuronal and glial apoptosis in human traumatic brain injury. *Int J Legal Med* (2007) **121**:365-375. doi: 10.1007/s00414-006-0126-6 [doi].

(38) Kelso ML, Gendelman HE. Bridge between neuroimmunity and traumatic brain injury. *Curr Pharm Des* (2014) **20**:4284-4298. doi: CPD-EPUB-55952 [pii].

(39) Jassam YN, Izzy S, Whalen M, McGavern DB, El Khoury J. Neuroimmunology of Traumatic Brain Injury: Time for a Paradigm Shift. *Neuron* (2017) **95**:1246-1265. doi: S0896-6273(17)30612-8 [pii].

(40) Czigner A, Mihaly A, Farkas O, Buki A, Krisztin-Peva B, Dobo E, et al. Kinetics of the cellular immune response following closed head injury. *Acta Neurochir (Wien)* (2007) **149**:281-289. doi: 10.1007/s00701-006-1095-8 [doi].

(41) Clausen F, Lorant T, Lewen A, Hillered L. T lymphocyte trafficking: a novel target for neuroprotection in traumatic brain injury. *J Neurotrauma* (2007) **24**:1295-1307. doi: 10.1089/neu.2006.0258 [doi].

(42) Fernandez-Klett F, Priller J. The fibrotic scar in neurological disorders. *Brain Pathol* (2014) **24**:404-413. doi: 10.1111/bpa.12162 [doi].

(43) de Vos AF, van Meurs M, Brok HP, Boven LA, Hintzen RQ, van der Valk P, et al. Transfer of central nervous system autoantigens and presentation in secondary lymphoid organs. *J Immunol* (2002) **169**:5415-5423.

(44) Urra X, Miro F, Chamorro A, Planas AM. Antigen-specific immune reactions to ischemic stroke. *Front Cell Neurosci* (2014) **8**:278. doi: 10.3389/fncel.2014.00278 [doi].

(45) Walsh JT, Zheng J, Smirnov I, Lorenz U, Tung K, Kipnis J. Regulatory T cells in central nervous system injury: a double-edged sword. *J Immunol* (2014) **193**:5013-5022. doi: 10.4049/jimmunol.1302401 [doi].

(46) Antila S, Karaman S, Nurmi H, Airavaara M, Voutilainen MH, Mathivet T, et al. Development and plasticity of meningeal lymphatic vessels. *J Exp Med* (2017) **214**:3645-3667. doi: 10.1084/jem.20170391 [doi].

(47) Arumugam TV, Granger DN, Mattson MP. Stroke and T-cells. *Neuromolecular Med* (2005) **7**:229-242. doi: NMM:7:3:229 [pii].

(48) Meisel C, Schwab JM, Prass K, Meisel A, Dirnagl U. Central nervous system injury-induced immune deficiency syndrome. *Nat Rev Neurosci* (2005) **6**:775-786. doi: nrn1765 [pii].

(49) Mazzeo AT, Kunene NK, Gilman CB, Hamm RJ, Hafez N, Bullock MR. Severe human traumatic brain injury, but not cyclosporin a treatment, depresses activated T lymphocytes early after injury. *J Neurotrauma* (2006) **23**:962-975. doi: 10.1089/neu.2006.23.962 [doi].

(50) Mrakovcic-Sutic I, Tokmadzic VS, Laskarin G, Mahmutefendic H, Lucin P, Zupan Z, et al. Early changes in frequency of peripheral blood lymphocyte subpopulations in severe traumatic brain-injured patients. *Scand J Immunol* (2010) **72**:57-65. doi: 10.1111/j.1365-3083.2010.02407.x [doi].

(51) Bigler ED. Neuroinflammation and the dynamic lesion in traumatic brain injury. *Brain* (2013) **136**:9-11. doi: 10.1093/brain/aws342 [doi].

(52) Schimmel SJ, Acosta S, Lozano D. Neuroinflammation in traumatic brain injury: A chronic response to an acute injury. *Brain Circ* (2017) **3**:135-142. doi: 10.4103/bc.bc_18_17 [doi].

(53) McKee CA, Lukens JR. Emerging Roles for the Immune System in Traumatic Brain Injury. *Front Immunol* (2016) **7**:556. doi: 10.3389/fimmu.2016.00556 [doi].

(54) Moalem G, Leibowitz-Amit R, Yoles E, Mor F, Cohen IR, Schwartz M. Autoimmune T cells protect neurons from secondary degeneration after central nervous system axotomy. *Nat Med* (1999) **5**:49-55. doi: 10.1038/4734 [doi].

(55) Schwartz M, Raposo C. Protective Autoimmunity: A Unifying Model for the Immune Network Involved in CNS Repair. *Neuroscientist* (2014) **20**:343-358. doi: 1073858413516799 [pii].

(56) Weckbach S, Neher M, Losacco JT, Bolden AL, Kulik L, Flierl MA, et al. Challenging the role of adaptive immunity in neurotrauma: Rag1(-/-) mice lacking mature B and T cells do not show neuroprotection after closed head injury. *J Neurotrauma* (2012) **29**:1233-1242. doi: 10.1089/neu.2011.2169 [doi].

Figure 1

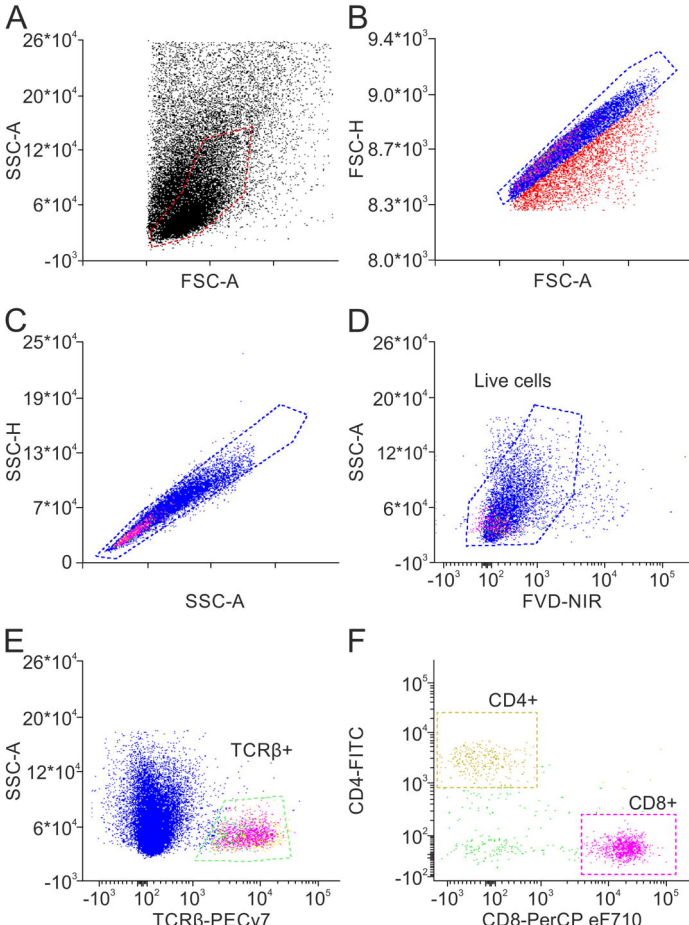
A
SSC-A
FSC-A
B
FSC-H
FSC-A
C
SSC-H
SSC-A
D
Live cells
SSC-A
FVD-NIR
E
TCRβ+
SSC-A
TCRβ-PECy7
F
CD4+
CD8+
CD4-FITC
CD8-PerCP eF710

Figure 2

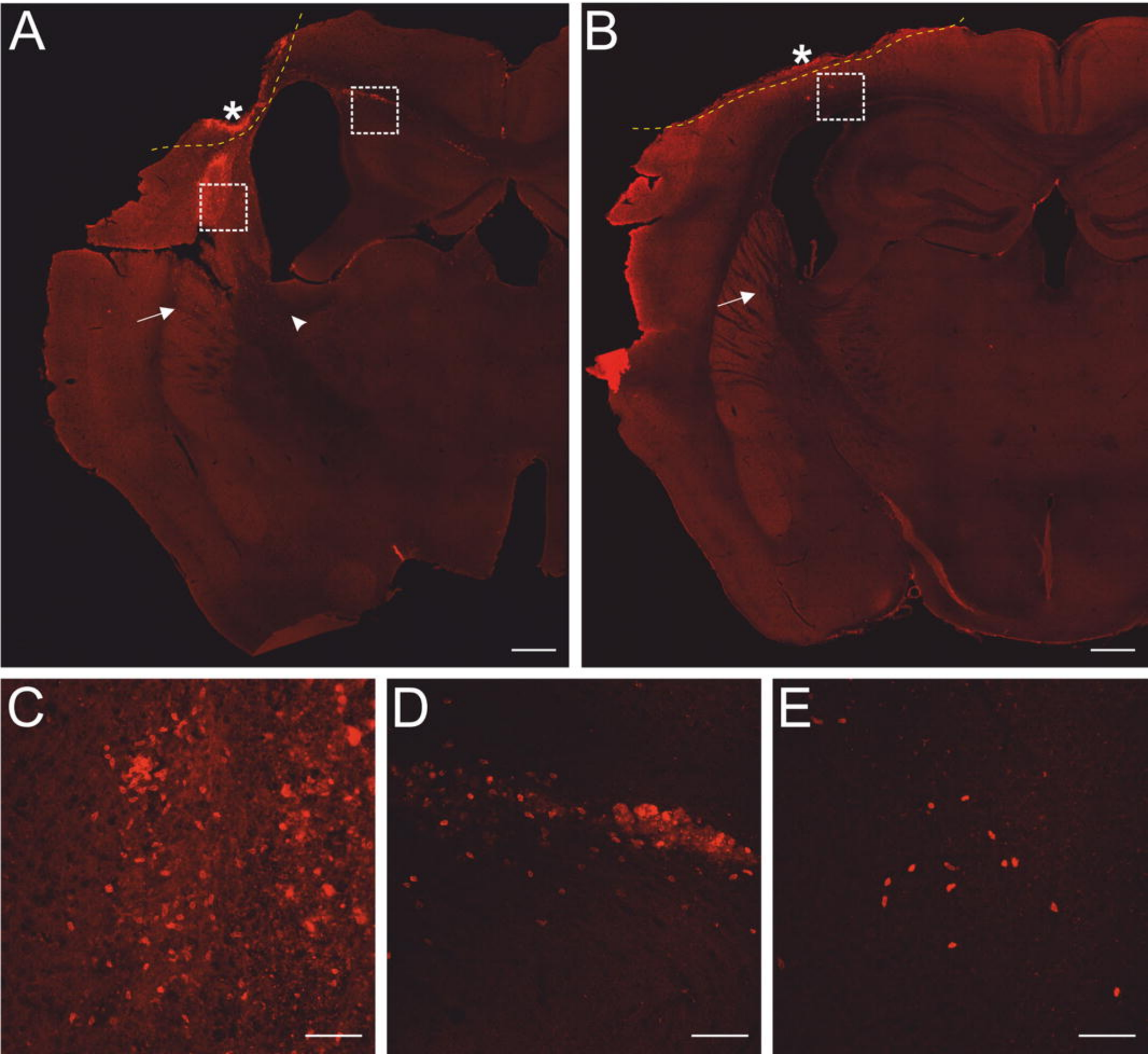

Figure 3

A

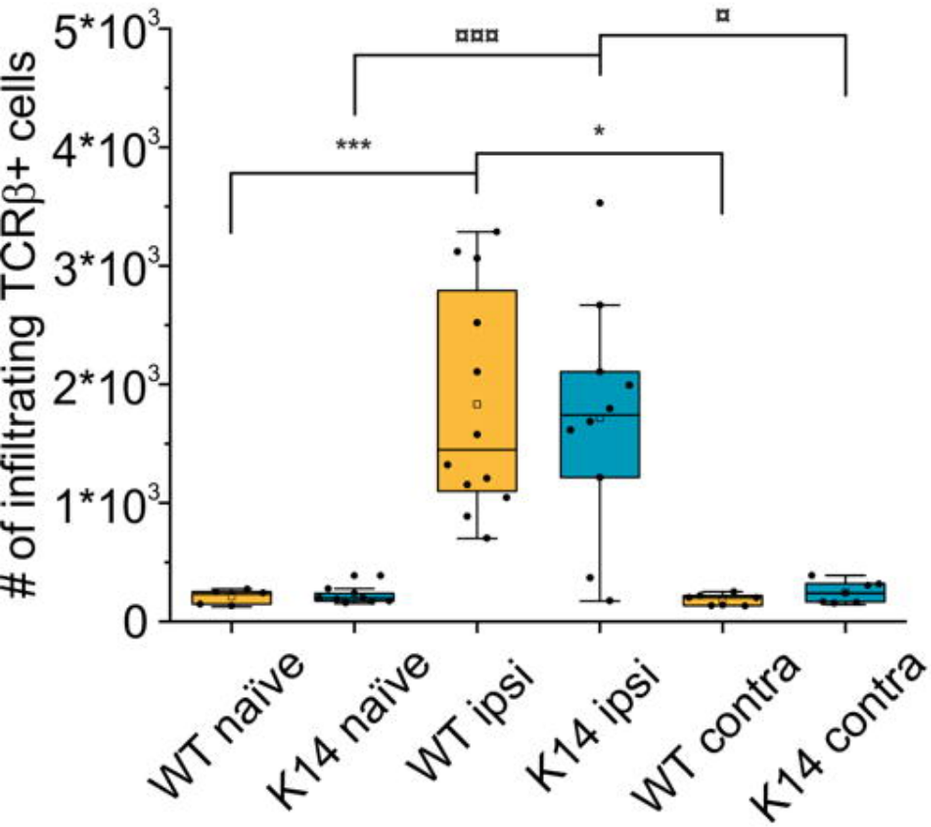

B

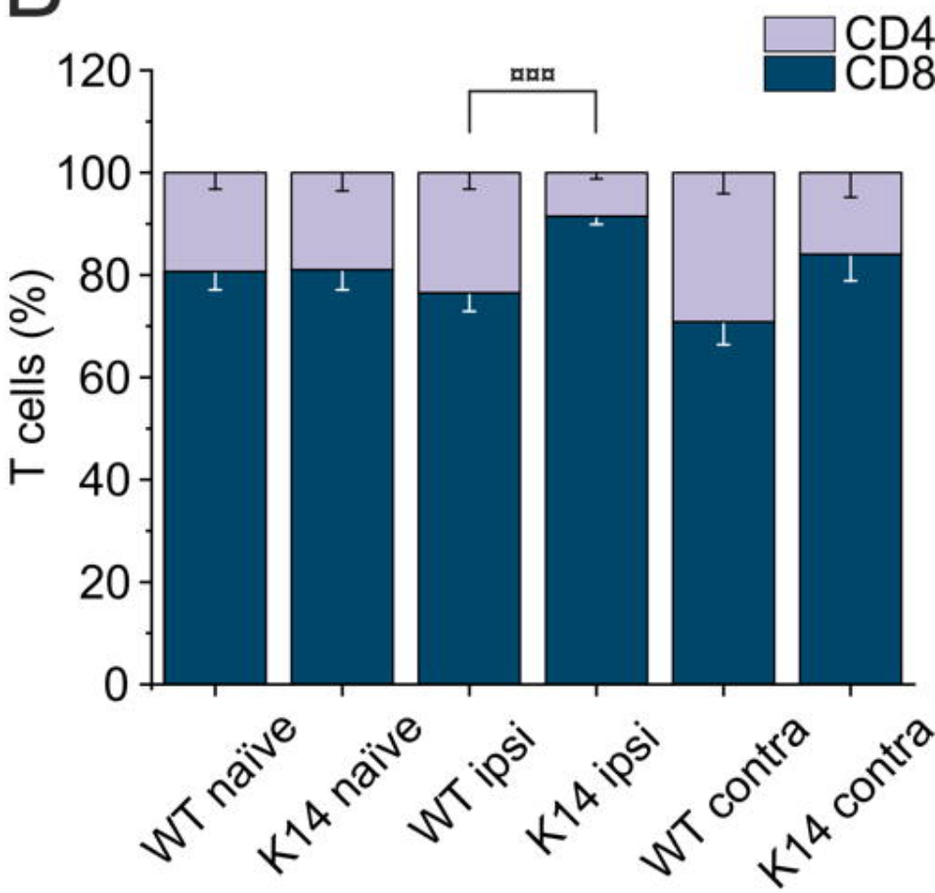

C

TCRβ+ cells (counts)					
Comparisons (within WT)	p-value	Comparisons (within K14)	p-value	Comparisons (between genotypes)	p-value
ipsi *vs.* naïve	<0.0001 (***)[a]	ipsi *vs.* naïve	<0.0001 (¤¤¤)[a]	naïve (WT *vs.* K14)	1.0000[a]
ipsi *vs.* contra	0.0112 (*)[b]	ipsi *vs.* contra	0.0151 (¤)[b]	ipsi (WT *vs.* K14)	1.0000[a]
contra *vs.* naïve	1.0000[a]	contra *vs.* naïve	1.0000[a]	contra (WT *vs.* K14)	1.0000[a]

[a] by Kruskal Wallis test, followed by Bonferroni correction
[b] by paired samples Wilcoxon signed rank test, followed by Bonferroni correction

Figure 4

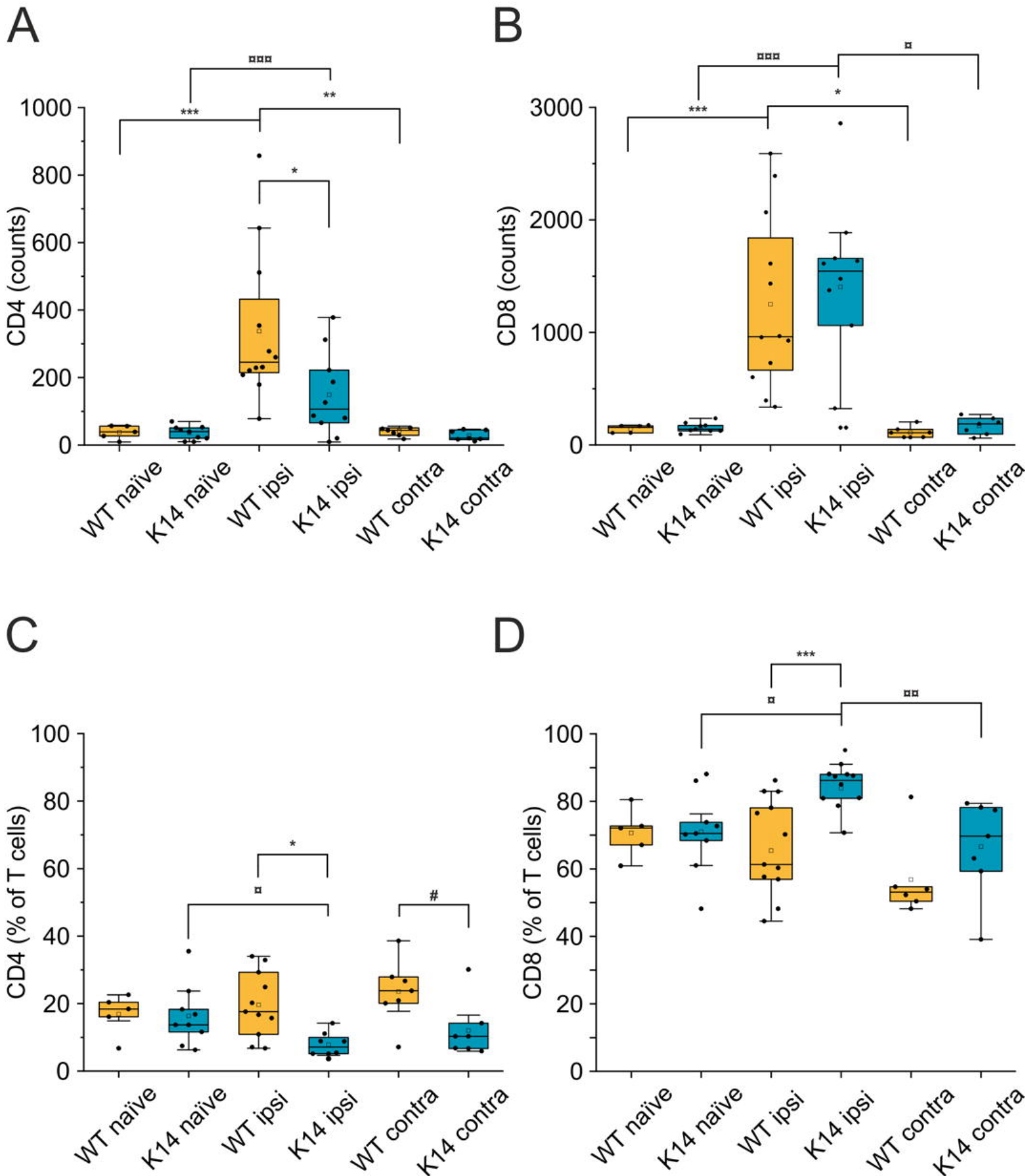
A
CD4 (counts)
1000
800
600
400
200
0
¤¤¤
***
**
*
WT naïve
K14 naïve
WT ipsi
K14 ipsi
WT contra
K14 contra
B
CD8 (counts)
3000
2000
1000
0
¤¤¤
¤
***
*
WT naïve
K14 naïve
WT ipsi
K14 ipsi
WT contra
K14 contra
C
CD4 (% of T cells)
100
80
60
40
20
0
*
¤
#
WT naïve
K14 naïve
WT ipsi
K14 ipsi
WT contra
K14 contra
D
CD8 (% of T cells)
100
80
60
40
20
0
***
¤
¤¤
WT naïve
K14 naïve
WT ipsi
K14 ipsi
WT contra
K14 contra

Figure 5

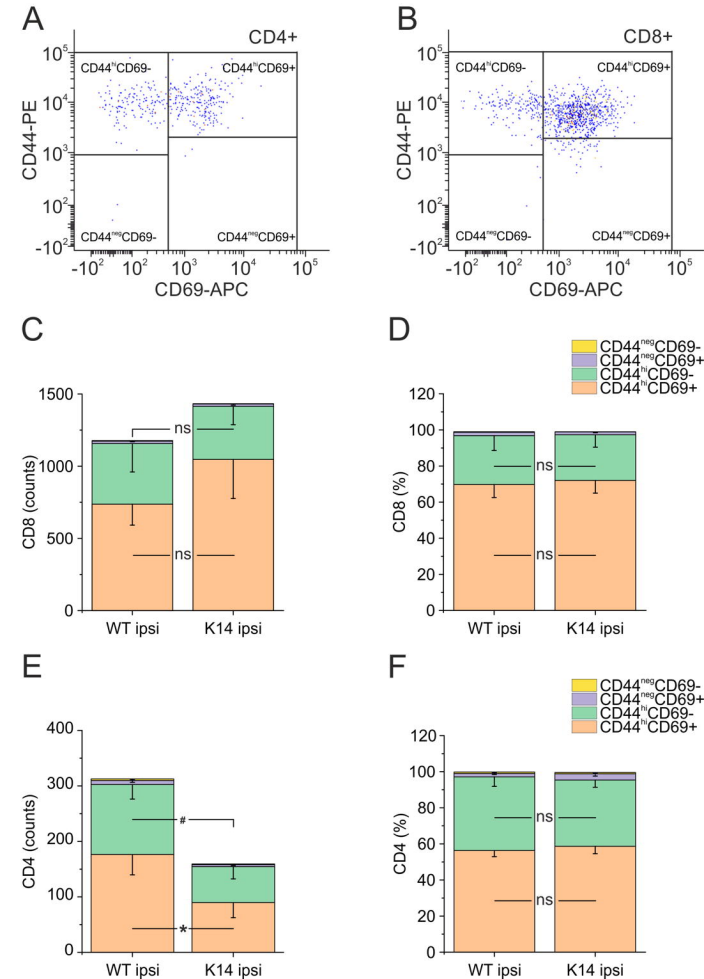
A
CD4+
CD44hiCD69-
CD44hiCD69+
CD44negCD69-
CD44negCD69+
CD44-PE
CD69-APC
B
CD8+
CD44hiCD69-
CD44hiCD69+
CD44negCD69-
CD44negCD69+
CD44-PE
CD69-APC
C
CD8 (counts)
ns
ns
WT ipsi
K14 ipsi
D
CD44negCD69-
CD44negCD69+
CD44hiCD69-
CD44hiCD69+
CD8 (%)
ns
ns
WT ipsi
K14 ipsi
E
CD4 (counts)
#
*
WT ipsi
K14 ipsi
F
CD44negCD69-
CD44negCD69+
CD44hiCD69-
CD44hiCD69+
CD4 (%)
ns
ns
WT ipsi
K14 ipsi

Figure 6

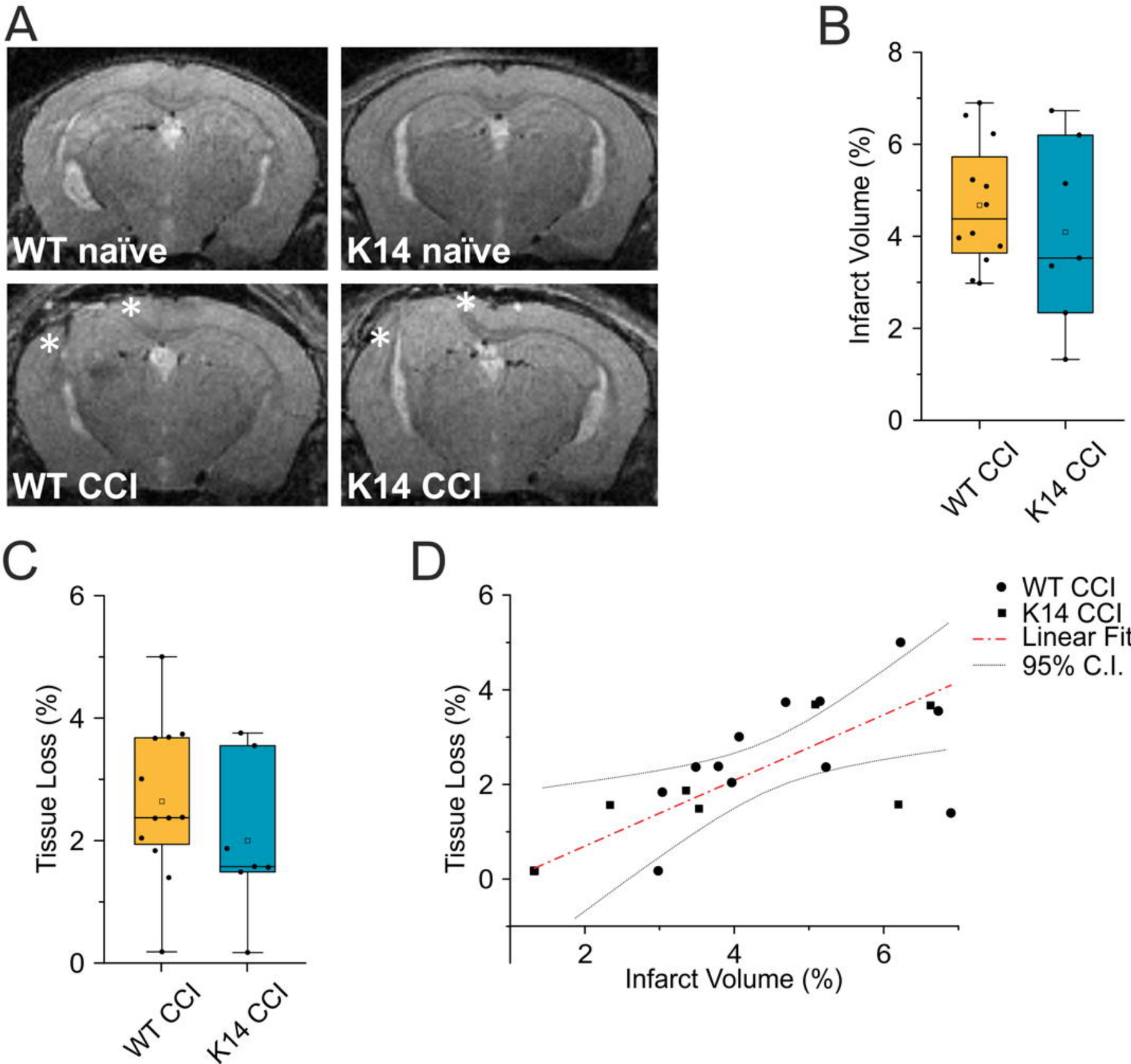
A
WT naïve
K14 naïve
WT CCI
K14 CCI
B
Infarct Volume (%)
0
2
4
6
8
WT CCI
K14 CCI
C
Tissue Loss (%)
0
2
4
6
WT CCI
K14 CCI
D
Tissue Loss (%)
Infarct Volume (%)
0
2
4
6
2
4
6
WT CCI
K14 CCI
Linear Fit
95% C.I.

Figure 7

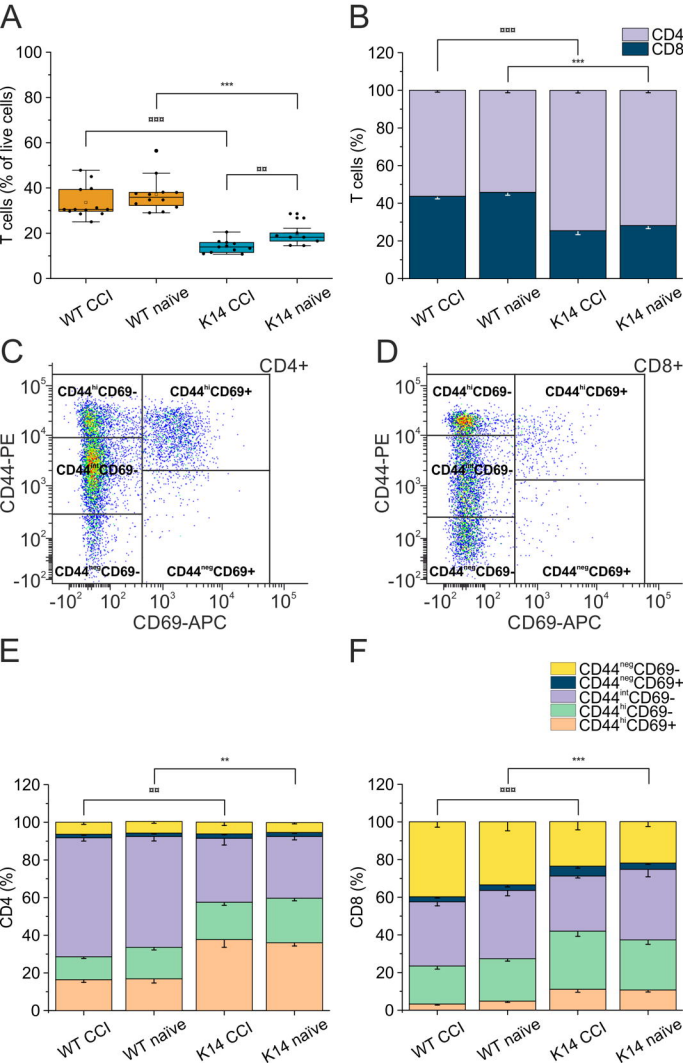
A
T cells (% of live cells)
WT CCI
WT naïve
K14 CCI
K14 naïve
B
CD4
CD8
T cells (%)
C
CD4+
CD44hiCD69-
CD44hiCD69+
CD44intCD69-
CD44negCD69-
CD44negCD69+
CD44-PE
CD69-APC
D
CD8+
E
CD4 (%)
F
CD44negCD69-
CD44negCD69+
CD44intCD69-
CD44hiCD69-
CD44hiCD69+
CD8 (%)